The topographic control on land surface energy fluxes

Alessandra Trevisan[a, *], Victor Venema[a], Stefan Kollet[b, c], Mostaquimur Rahman[a, I]

[a] Meteorological Institute, University of Bonn, Germany

[b] Agrosphere Institute, Research Centre Juelich, Germany

[c] Centre for High-Performance Scientific Computing in Terrestrial System, Geoverbund, ABC/J, Germany

[I] present address: Department of Civil Engineering, University of Bristol, UK

[*]Corresponding Author: A. Trevisan, trevisan@uni-bonn.de

Abstract

Subsurface hydrodynamics are an important component of the hydrological cycle and a key factor in the partitioning of the land surface energy fluxes. Because also of computational reasons they are often neglected, or strongly simplified, in numerical weather prediction and climate models. Particularly in regions where the water table is shallow, soil moisture acts as a link between land, atmosphere and groundwater and, because of its long-term memory represents a buffer for the effects of climate variability. To dynamically model this system we couple a variably saturated groundwater flow model (ParFlow) with a surface model (CLM). In order to overcome the computational limitations of such an explicit representation of the groundwater dynamics, we propose an approach for the statistical correction of the bias of the energy fluxes of a simple scheme, based on the comparisons with fully-coupled subsurface-land-atmosphere simulations. This simple dynamical scheme computes the potential latent heat flux in case of near saturation. In particular, we focus on the ability of topography-related indices, such as the topographic wetness index and the depth-to-water index, to provide information on the availability of water for evapotranspiration. The topographic indices confirm to be good predictors for the moisture availability. While the small scale structure cannot be captured well, the results show that the large-scale biases of latent heat flux over the domain are effectively removed. Moreover, the bias corrected fluxes more accurately reproduce the fluxes of the full modelling system than common used free drainage simulations. Thus, the proposed approach can be useful in approximating the effect of groundwater on land surface water and energy fluxes in e.g. regional climate models.

1 Introduction

Groundwater is the primary source of fresh water (*Gleick*, 1993) and a major source of water supply for consumption, agriculture and industry. As an important element of the hydrologic cycle, groundwater sustains surface waters, ecosystems and the aquatic communities that populate these areas (*Alley et al.*, 2002, *Fan and Miguez-Macho*, 2010). In the areas where soil moisture is the limiting factor for the evapotranspiration, capillary rise from the groundwater table may result directly into enhanced evapotranspiration (*Anyah et al.*, 2008) and decreased infiltration (*Yeh and Eltahir*, 2005a). The water table depth (wtd) is a function of groundwater dynamics and surface fluxes, such as evapotranspiration and infiltration in the unsaturated zone (*York et al.*, 2002) and affects the soil moisture profile at different space and time scales (*Vergnes et al.*, 2012). This is reflected in the partitioning between surface and subsurface soil water and the partitioning between surface sensible and latent heat fluxes, which affects the terrestrial water and energy balance and the atmospheric processes (*Choi and Liang*, 2010, *Leung et al.*, 2011).

The influence of groudwater storage on the energy and water exchanges between soil and atmosphere can be conceptually understood for an idealized hillslope. The hillslope is assumed to be divided into three regions with deep (C), intermediate (B) and shallow (A) groundwater table (*Kollet and Maxwell*, 2008). Assuming that the water table follows the topography (a simplification that is generally true for topographically driven groundwater flow), it is deeper for the hill tops and shallower in the valleys, thus the three zones correspond to three conceptual soil columns, that are connected by lateral groundwater flow. In case A, where the water reaches or is close to the surface, the surface processes are not water limited and small variations in water table depth do not affect the land surface processes. In case C, the water can only drain downwards (groundwater recharge) and there is no significant linkage between water table depth and land surface processes. Finally, in case B, which corresponds to the transition between the two regimes, the groundwater is at a "critical depth", i.e. small changes in depth can alter the water availability for evaporation and root water uptake, allowing the vertical redistribution of soil moisture. This implies that in case B, there is a connection between groundwater and land surface related to the location of the water table and, thus, to the availability of water, which affects the energy fluxes (in particular the partition of energy between sensible and latent heat). In this regime it is therefore most important to model the position of the groundwater table and its evolution over time accurately.

This subdivision in three regimes was reflected in the relationship between latent heat and depth to groundwater found in simulations (*Soylu et al.*, 2011, *Kollet and Maxwell*, 2008) and was also confirmed in measured data (*Szilagyi et al.*, 2013). They show nearly no dependence of the fluxes on *wtd* for deep and shallow water tables (case A and case C), while for the intermediate region (case B) the curve is steep, implying that small changes in groundwater table influence the energy fluxes. The depth of this critical zone is also determined by the plant rooting depth (*Fan*, 2015). While this relationship between energy fluxes and water table depth is generally present in the critical zone, its strength can vary, depending on the soil composition and the land use type (*Maxwell et al.*, 2007, *Kollet and Maxwell*, 2008).

Despite the importance of groundwater dynamics for climate, the subsurface in *LSMs* is commonly represented by single soil columns. Moreover, a free drainage boundary condition at the bottom of the column is often used, which implies a negligible upward diffusive flux (*Yeh and Eltahir*, 2005b), even for regions of the domain where the water table is shallow in reality. This means that the lateral movement of water between the columns is neglected and water is lost, instead of being laterally distributed towards the neighbouring columns, causing a bias in the mass and energy balance (*Tian et al.*, 2012, *Miguez-Macho et al.*, 2007).

In the last decades a number of studies, which are briefly reviewed below, demonstrated the importance of subsurface hydrodynamics for climate and weather modelling. The Land Surface Models (LSMs) provide the lower boundary condition for temperature and moisture in the General Circulation Models (GCMs), the mesoscale Regional Climate Models (RCMs) and the Numerical Weather Prediction models (NWPs). They describe the water and energy fluxes on the land surface, and the partitioning of the incoming precipitation into surface and subsurface runoff, evapotranspiration (ET) and soil moisture variation, but their description of the subsurface hydrodynamics is often highly simplified (*Tian et al.*, 2012). Several studies on the coupling of a groundwater component in *LSMs* showed that the inclusion of a dynamical representation of water table modifies the vertical profile of soil moisture and improves the water budget simulation (e.g., *York et al.*, 2002, *Maxwell and Miller*, 2005, *Jiang et al.*, 2009, *Lo and Famiglietti*, 2011, *Leung et al.*, 2011). Over short time scales and at the catchment scale, *Maxwell et al.* (2007) showed that a more realistic soil moisture distribution is obtained with the inclusion of the groundwater and that this affects the local atmospheric convection. *Miguez-Macho et al.* (2007) showed that the presence of the water table as the lower boundary of the soil causes a slower vertical drainage, that concurs with the upward capillary flux and the lateral groundwater convergence to the increase of soil moisture in the root zone, compared to a free-drainage run. In areas where the water table is deep, variations in land surface energy fluxes mostly depend on the precipitation (*Maxwell and Kollet*, 2008) and the free (gravity) drainage assumption is reasonable, since the saturated and unsaturated zones of the subsurface are not interacting (*Vergnes et al.*, 2014, *Lo and Famiglietti*, 2010). When the water table is shallow, which is the case for almost 50% of the global land according to simulations (*Koirala et al.*, 2014), the upward flux from the aquifer to the shallow soil compartment and the decrease in infiltration (*Yeh and Eltahir*, 2005b) affect the seasonal precipitation and temperature (*Jiang et al.*, 2009, *Anyah et al.*, 2008, *Maxwell and Kollet*, 2008, *Betts*, 2004).

In a study on the strength of the interactions between land and atmosphere, *Lo and Famiglietti* (2011) found that the effect of the groundwater on precipitation varies globally. In areas where the subsurface and atmosphere are strongly coupled, the groundwater presence enhances shallow soil moisture, which is transported vertically via evapotranspiration, impacting the initiation of convection. The augmented precipitation induces a positive feedback, where the wetter soil produces more evapotranspiration. Therefore, wet areas may get wetter and arid regions may get drier (*Chou and Neelin*, 2004).In reality, this rule of thumb for the expected trend in climate change is, however, extremely reductive and evidence of the opposite trend has been found, especially on land surfaces (*Greve et al.*, 2014).

In a comparison of two runs of a regional model with and without aquifer over a catchment in northeastern Kansas, *York et al.* (2002) found that between 5% and 20% (for wet and dry years, respectively) of ET comes from the aquifer. In a similar fashion, *Niu et al.* (2007) compared two experiments with free drainage and groundwater recharge as lower bondary condition, finding that the latter produces 4% to 16% (depending on the region) more annual evapotranspiration, with the transitional arid-to-wet areas presenting the largest effect of wetter soil on ET. Especially during dry periods, a shallow water table can sustain ET and reduce the sensitivity of surface soil moisture to precipitation anomalies (*Vergnes et al.*, 2014, *Yeh and Eltahir*, 2005a). Conversely, in areas with deeper groundwater table the soil moisture is more sensitive to anomalies in precipitation, which result in stronger fluctuations in the evaporative fraction (*Leung et al.*, 2011).

The variations in the fluxes of energy and moisture affect precipitation (*Anyah et al.*, 2008) directly through convection or indirectly through advection, encreasing the spatial scale of the influence of groundwater on the atmosphere (*Yuan et al.*, 2008). According to *Lam et al.* (2011), groundwater can locally contribute more than 30% of evaporation in summer and increase the multi-year memory of climate models, by a sustained influence of wet episodes for several years. The water table acts as a buffer for the temporal variations of the soil moisture, due to its slow changing nature (*Miguez-Macho et al.*, 2007, *York et al.*, 2002) and reduces the impact of drought in forested regions (*Decker et al.*, 2013). As the atmospheric forcing propagates through the land surface hydrologic cycle, its anomalies persist in the water table levels, due to the longer memory of groundwater compared to soil moisture; they are then transported upward and impact the future climate (*Yeh and Eltahir*, 2005a). The ability of the land surface to respond to anomalies in the climate is obviously affected by land use change (*Leung et al.*, 2011) and the water table position responds also to the depletion caused by groundwater pumping (*Leng et al.*, 2014), so the anthropogenic influence alters significantly the hydrologic cycle (*Ferguson and Maxwell*, 2010).

As discussed above, groundwater hydrodynamics are a key factor in influencing the energy fluxes at the land surface, yet a full three-dimensional subsurface representation is computationally not feasible in global climate simulations. To overcome this limitation we propose a Model Complexity Reduction Approach (*MCRA*), connecting a parameterized groundwater representation for large scale models, with small-scale physics based simulations. In the MCRA most of the surface physics is modelled by a dynamical model and bias-corrected with a simple statistical model. The reverse approach was used for fast and accurate modelling radiative transfer in atmospheric models (*Venema et al.*, 2007; *Manners et al.*, 2009; *Schomburg et al.*, 2012). In these radiative transfer schemes, the simpler physical or statistical model was responsible for efficiently modelling the small-scale variability, while the complex physical model was used to reduce biases.

The approach is based on two sets of simulations. A full-physics simulation, *CplxRun*, represents the virtual reality, while a highly parameterized simulation, *LandParm*, is used as a reference. For this study, a Potential Latent Heat Run (*PotLERun*) is used as parameterized simulation. In it, the water table depth is fixed at the soil surface, as opposed to the *CplxRun*, where the water table is free to move in response to atmospheric forcing and topographic characteristics.

Topographic indices, such as Depth-To-Water and Topographic Index, effectively represent the relative abundance of water at different locations in the watershed. Based on the fact that evapotranspiration is constrained by the availability of water and radiation, we will develop a statistical model for the correction of the *PotLERun*, in order to approximate the results of the *CplxRun*. The validity of the concept and the ability to correct the latent heat flux will be demonstrated using cross-validation in space.

The paper is structured as follows: in the first part we present the methodology. The Model Complexity Reduction Approach is described as a general concept, followed by the simulations that this work is based on are then illustrated, starting with the model used to perform them. In section 2.4 the topographic indices used in the bias correction are presented and the sensitivity of the latent heat flux to these indices and to other static parameters is shown. Finally, the statistical bias-correction model is explained, tested in a cross-validation and compared to a free drainage simulation.

2 Methodology

In this section, we present the Model Complexity Reduction Approach, the adaptive parameterization that is the core of this work. We then introduce the simulation data, starting from the numerical model used to obtain them (Section 2.2). The general characteristics of the domain are presented in Section 2.3, with a particular focus on possible key parameters for a statistical model for energy and moisture fluxes. The data originate from a previous study, *Rahman et al.* (2014), where more details can be found.

2.1 Model Complexity Reduction Approach, MCRA

A Model Complexity Reduction Approach (*MCRA*) is proposed (Figure 1), where a fast simplified model (*LandParm*) is run over the whole domain. Because of the simplifications, LandFast is biased. These biases are corrected statistically (bias corrector). The biases are estimated by comparing LandFast outuput to the results of a full complex model system (*LandCplx*) simulations. In the *Updater* all the information is collected and elaborated, in order to provide the updated values of spatially averaged latent heat, serving as lower boundary flux for *GCMs* and *RCMs*. The information is represented by static parameters used as predictors and the results of the full complex model system (*Landcplx*) simulations.

In this study the *MCRA* adaptive approach is implemented using a LandFast simulation where the water table was fixed at the surface and the source/sink term turned off, to simulate a full availability of moisture (Potential Latent Heat Run, *PotLERun*), while the rest of the setup (e.g., resolution) is identical to the Complex Run. Because the soil is saturated, the computationally expensive

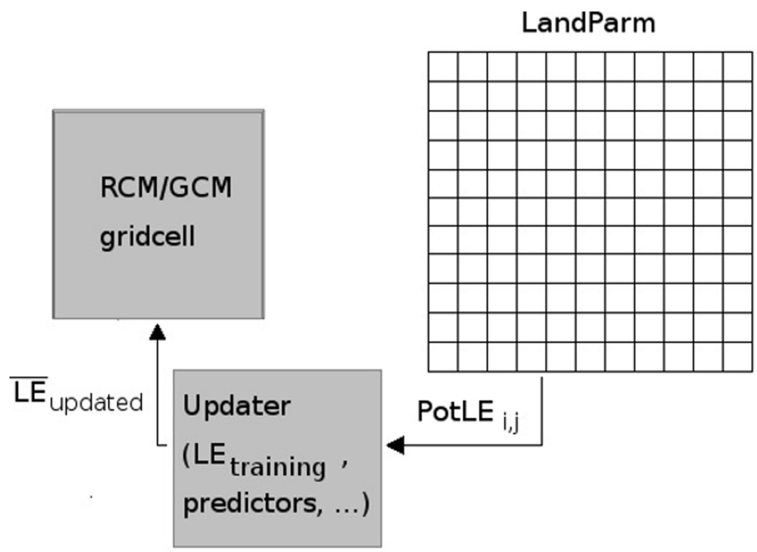

Figure 1. Scheme of the MCRA concept.

flow of water does not need to be simulated. This allows a reduction in the run time, that is estimated to be 1/15 of the standard run time for *CplxRun*.

The data for training the scheme are produced by a Complex Run (*CplxRun*), where the subsurface hydrodynamics is fully simulated and the water table is free to move.

We will develop a statistical model for the difference between *CplxRun* and *PotLERun* to function as the updater. Because *PotLERun* already includes much physics, the statistical model can be much more parsimonious than a full statistical model for the surface fluxes, and only focuses on correcting for the over abundance of soil moisture. Since the *PotLERun* does not provide a physically consistent water table depth, the topographic indices, that are proxies of the wetness of the soil, are used as predictors in the statistical model for the difference in evapotranspiration between the two runs,ΔLE.

The advantage offered by the use of simulations instead of measurements is the full availability of hourly data for the variables and full control on the static parameters. The goal of this study is thus to develop a fast surface parameterisation that mimics LandCplx as well as possible.

For each class, the behaviour is assumed to be consistent and on average the same in the validation and in the training set. The predicted value for the latent heat, $LE_{pred,i}$, in each cell i of the class is calculated as the difference between the value of $LE_{pot,i}$ and the corresponding ΔLE, δ_i:

$$LE_{pred,i} = LE_{pot,i} - \delta_i \tag{1}$$

The value of δ_i is unknown during the prediction phase. It is approximated with the average ΔLE of the same class, as calculated in the training set, $\overline{\delta_{train}}$:

$$LE_{pred,i} = LE_{pot,i} - \overline{\delta_{train}} \tag{2}$$

In this way the error in the prediction for each cell is equal to the difference between the true value of ΔLE in the cell and the mean value of it for that class. The bias is then:

$$\overline{(LE_{pred,i} - LE_{true,i})} = \overline{(\delta_i - \overline{\delta_{train}})}, \tag{3}$$

meaning that if the residuals of the ΔLE values are homogeneously distributed, the bias will be small and the spatial mean of predicted latent heat will be a good approximation of the true value.

2.2 ParFlow.CLM

ParFlow is a variably saturated groundwater flow model with an integrated overland flow simulation capability. It has been coupled with *CLM* (Common Land Model) to incorporate physical processes that are related to the balances of energy and water at the land surface (*Maxwell and Miller*, 2005, *Kollet and*

Maxwell, 2006, 2008). *CLM* calculates the mass and energy balance at the land surface, in terms of evaporation from canopy and ground surface, transpiration from plants, ground heat flux, freeze-thaw processes and sensible heat fluxes. *ParFlow* replaces the soil column formulation and runoff scheme of *CLM*. The coupling between the two models is performed via soil moisture, evapotranspiration and infiltration of water. The atmospheric forcing can be represented by reanalysis data or the results from an atmospheric model.

2.3 The simulations

The analysis deals with the results of two *ParFlow.CLM* simulations (from now on, the *CplxRun* and the *PotLERun*) performed over a domain that includes the Rur catchment (*Rahman et al.*, 2014). The spatial resolution is $\Delta x = \Delta y =$ 1 km and the domain includes 168×168 cells. The soil is subdivided in layers, the thickness of which is increasing with depth (it varies from 0.04 m for the uppermost layer, to 4 m for the deepest one) in order to better resolve the dynamics in the shallow subsurface. The outputs consist of two-dimensional hourly data for the energy fluxes at the surface and three-dimensional hourly data for saturation and pressure in the subsurface, that span one year (namely 2009). The water table depth is calculated based on the pressure profile in the subsurface, for each cell in the domain and each time step of the simulation. Positive values indicate cells where the groundwater table is below the surface, while negative values correspond to ponded water. The depth varies in time in response to the atmospheric forcing (*Rahman et al.*, 2014) and in space according to the hydraulic properties, gravity and pressure driven fluxes.

The domain encompasses a variety of land uses and soil textures (Figure 2). The land use classification follows the GLC2000 dataset (*Skalsky et al.*, 2009). The domain shows a large area of mostly natural vegetation in the southern

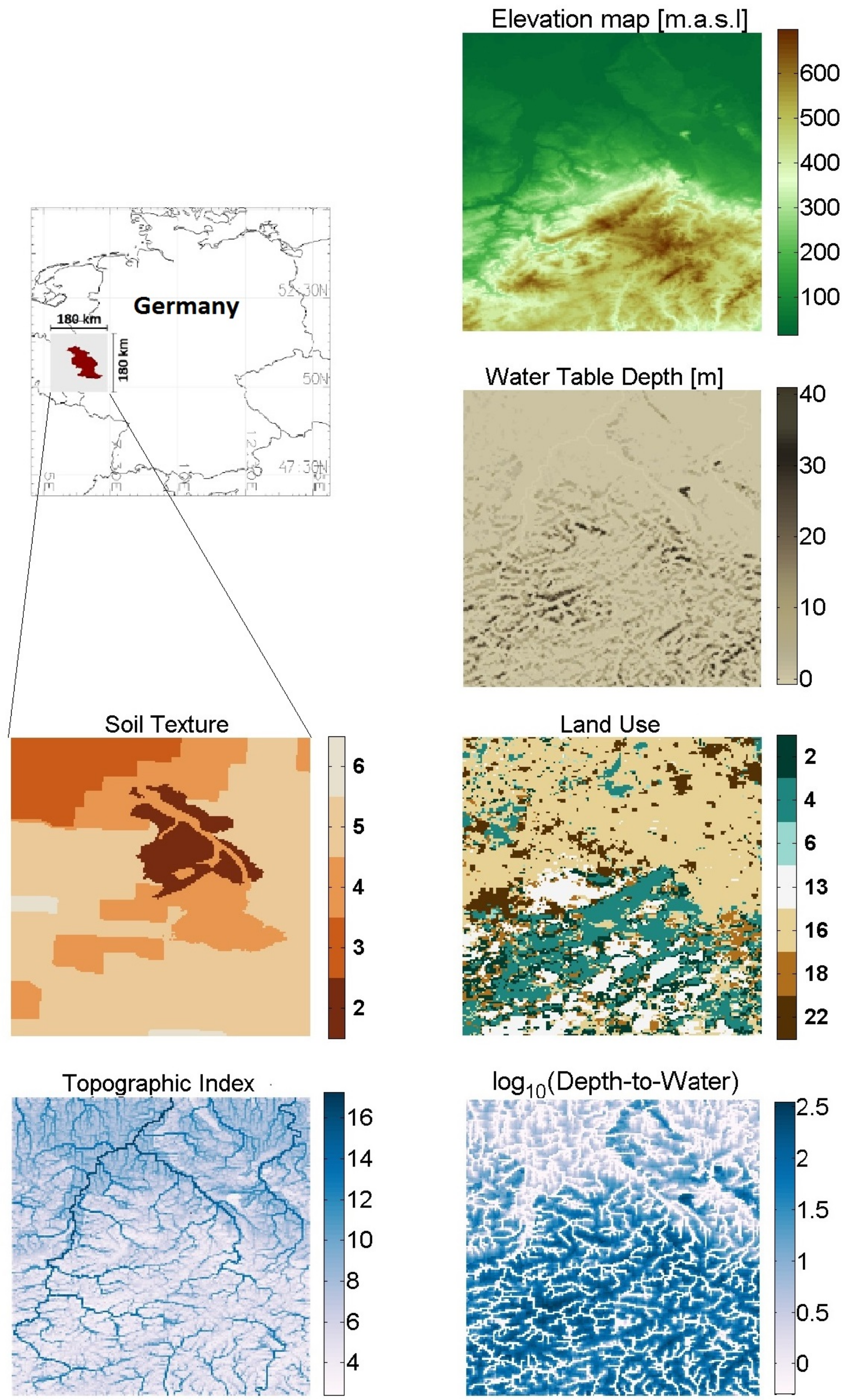

Figure 2. Overview of the topographic and surface characteristics of the domain. For the land use map, the correspondence is: 2) broadleaved deciduous trees; 4) needle-leaved evergreen trees; 6) mixed leaf type trees; 13) herbaceous cover; 16) cultivated and managed areas; 18) mosaic: cropland/shrub or grass cover; 22) artificial surfaces and associated areas. For the soil texture, the correspondence is: 2) silty clay; 3) loamy sand; 4) silt loam; 5) clay loam; 6) silt.

mountainous part, in correspondence to the Eifel National Park, while the northern part is mostly covered by cultivated and managed areas. With regard to the soil texture, silt is only present in two small areas, while clay loam represents the most abundant soil type. Silt loam is present in both the mountainous and the flat areas. Conversely, loamy sand is only present in the flat area. The Rur catchment area mostly presents silty clay in the flat part and silt loam in the mountains.

For the first simulation, the *CplxRun*, the subsurface hydrodynamics is allowed to vary dynamically, in response to the spatial heterogeneity and the atmospheric forcing. The setup for the second simulation, the *PotLERun*, only differs from the *CplxRun* for the fact that the whole domain is kept close to saturation by prescribing the pressure in the subsurface. The potential evapotranspiration is defined as "the rate at which evapotranspiration would occur from a large area completely and uniformly covered with growing vegetation, which has access to an unlimited supply of soil water" (*Dingman*, 2002). This is the state which is simulated and which names the PotLERun. It represents a measure of the demand of water from the atmosphere that the soil can fully meet only if it is never water limited, as is the case in this simulation.

In this case the *CplxRun* represents the virtual truth, while the *PotLERun* is Landparm, a numerically efficient parameterization providing insight on the behaviour in case of extreme wetness.

The area is then split into a training and a validation subset. For the training set, both the results from *CplxRun* and *PotLERun* are used to develop the statistical model. The model is then tested on the validation set, by correcting the results of PotLERun, and comparing the corrected values against the *CplxRun* results.

2.3.1 Statistical model

The diurnal cycle on one subset was fitted with a modified Gaussian function,

$$F(t) = A_0 + A * \exp[\frac{-(t-t_0)^2}{2 * w}] \tag{4}$$

using an offset A_0, the difference between the maximum and minimum values as height A, $t = 13$ as the central hour, t_0, and a width, w, of 7 hours, for each class of the topographic index. The parameters were estimated by means of a dummy distribution with the same shape as the diurnal cycle over the month of July (where the bell is more pronounced) and checked on the other months.

2.3.2 Validation method

In order to demonstrate the ability of the topographic indices to quantify the ΔLE, the following procedure was applied. The entire domain was subdivided into two subsets, one for the training and one for the validation of the method. For the training data, the information coming from the *PotLERun* and the characteristics of the cells (e.g., the topographic indices) were used as predictors to develop a model for ΔLE. For validation, the outputs of the *CplxRun* were used.

The two subsets are organized in a "checkers" scheme (Figure 3), where the dark squares represent the training data and the whites are the validation, and vice versa. To ensure independence, the size of the squares needs to be large enough, thus the correlation length of the ΔLE was estimated. The analysis of the variogram shows it to be no larger than 5 km, which means that squares of 21 km of side length are a reasonable choice.

The comparison against a free-drainage (*FD*) simulation (*Rahman et al.*, 2016) serves as a second method of validation. In the *FD* simulation, the moisture is drained by gravity through the bottom of the domain, as opposed to

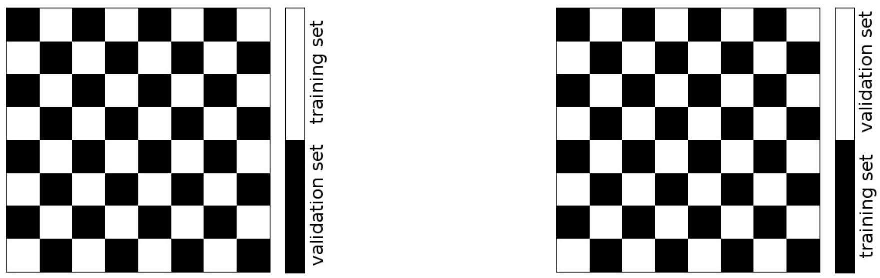

Figure 3. Training and Validation set 1 (left) and Training and Validation set 2 (right). The domain is subdivided into two subsets, according to a checkers scheme, that are used as training and validation set.

being redistributed in the subsurface according to the slopes. This boundary condition, commonly applied in land surface models, is known to have a "dry bias" due to the loss of water from the bottom of the column.

2.4 Topographic indices

2.4.1 Topographic Wetness Index

The *topographic index (TI)*, also called *wetness index*, was introduced in 1979, in the framework of the TOPMODEL approach (*Beven et al.*, 1984, *Beven and Kirkby*, 1979). It is defined as

$$TI = ln\left[\frac{\alpha}{\tan\beta}\right], \tag{5}$$

where the local slope β [-] is derived from the digital elevation model (DEM) and the specific catchment area α [m], is the area from which the water drains through the cell under investigation (contributing area), divided by the contour length. In equation 5, the slope determines the celerity of the runoff, while the contributing area is a measure of the potential amount of water. The *TI* represents an indicator of topographic heterogeneity in the catchment. It provides general information about shallow groundwater levels, at least in zones where these are mainly determined by topography and, thus, may be an indicator of the availability of water for evapotranspiration. In the last decades, the topographic index has been widely used as an index of hydrological similarity, under the assumption that points of a catchment with the same value of TI behave similarly, from the hydrological point of view (*Beven*, 1997). In summary, the topographic index formulation is based on some general assumptions (*Beven*, 1997, *Ducharne*, 2009, *Franchini et al.*, 1996) that are:

1. the local slope is a good approximation for the hydraulic gradient;
2. the dynamics of the water table can be approximated by a succession of steady states, in which an immediate balance between the local outflow from the saturated zone and the recharge from the contributing area is achieved at every time step and in every cell; and
3. the transmissivity of the soil declines exponentially with depth.

The validity of these assumptions varies between catchments and climates. If groundwater levels change slowly over time, for example, successive steady states represent the dynamics adequately (*Rinderer et al.*, 2014).

Alternative and more complex indices have been proposed and used (*Hjerdt et al.*, 2004, *Western et al.*, 1999), such as the soil-topographic index (*Beven*, 1986) and the climato-topographic index (*Merot et al.*, 2003), which include information about the transmissivity and the volume of annual effective rainfall, respectively. This is mainly necessary when a comparison between catchments with different characteristics, e.g., a different climatology, is performed or when the relaxation of some of the assumptions is necessary. For the purposes of this work the basic formulation is used.

The topographic index is computed from the slopes, with an algorithm that calculates the path of the water based on the maximum slope at every point and counts the contributing cells for every pixel. The higher values of topographic index correspond with the river channels (cells that receive the largest contribution from the catchment), while low values of TI are characteristics of cells that receive small contributions in, e.g., headwater catchments.

2.4.2 Depth-to-Water Index

An alternative topographic index is represented by the Depth-to-Water (DTW) index. It is a measure of the difference in elevation between each cell and the closest river cell which it is most likely hydrologically connected to (*Murphy et al.* (2009); *Rennó et al.* (2008) presents a different formulation, but an analogous concept).

Murphy et al. (2009) start from the DEM-derived slope and a flow-channel grid. An iterative function selects for every cell in the domain the nearest surface water cell and calculates the path that connects the two cells. This is then multiplied by the grid cell size, therefore approximating the total difference in elevation between each cell and the corresponding river cell. In this way, to each cell is assigned the value of

$$DTW = \left[\sum \frac{dz_i}{dx_i} a \right] x_c \tag{6}$$

where $\frac{dz}{dx}$ [-] is the local slope, i indicates the cell along the path, a is a coefficient that takes into account the direction of the flow across the cell (it is 1 when the flow is parallel to the grid lines and $\sqrt{2}$ when the flow is diagonal) and x_c [m] is the cell size (*Murphy et al.*, 2011). The river network highly influences the values and the pattern of the index. Generally, the hydrographic information on the area are used to determine wheter a cell belongs to the river network or not.

Low values of DTW indicate the tendency to have water at or near the surface, while drier areas have higher values, indicating a longer distance from the saturated areas (*Murphy et al.*, 2007). In the river channels, the DTW is zero by definition. Since the value assigned to each cell is the difference in elevation between that point and the associated river cell, the DTW index represents the elevation normalized with respect to the river network and corresponds to the relative position of the cell with respect to this datum.

The DTW index is also calculated from the slopes, with an algorithm that follows the flow of water (downslope) from each cell to the nearest (in the least cumulative slope sense) river cell. The value associated to each cell is the sum of the slope along the path, multiplied by the size of the cell, which yields the difference in elevation between them.In our implementation of the algorithm, only flow directions parallel to the cell borders are allowed ($D4$); the coefficient α is always 1. The cells are defined to be river cells according to a threshold in contributing area, which is also calculated based on the slopes. In order to ensure consistency, a comparison to the map of the rivers in the area and to the values of the average water table depth obtained from the simulation was performed. A threshold of 20 cells corresponding to $20\,\mathrm{km}^2$ was found to be satisfactory.

3 Results and discussion

3.1 Exploratory analysis of data

In this section, the analysis of the results of the above mentioned simulations is presented, with a particular focus on the influence of soil composition and land use on the energy fluxes, and on the relation of the different variables with the topographic indices.

In the first part, the relationship between the latent heat flux and water table depth is depicted. The two topographic indices, which will be used as predictors in the statistical model, are then briefly discussed and analyzed. For comparison, the relationship of latent heat flux with soil texture and land use are presented. Finally, the difference in latent heat flux between the two sets of simulations is analyzed, with respect to the predictors and other parameters, such as the land use and soil composition. The analyses focus mostly on the summer months and central hours of the day, since the difference in latent heat due to soil moisture limitations is expected to be largest in these times, in the study region (*Rahman et al.*, 2014).

3.1.1 Relationship of the latent heat flux to the water table depth

For the purpose of this analysis, the yearly average of water table depth is considered, in order to emphasize the relation to static parameters, such as the topographic indices.

Figure 4 shows the scatter plot of the monthly average latent heat flux (for the month of July) versus the water table depth, coloured according to land use (top) and soil texture (bottom). A typical pattern is present (see, e.g., *Szilagyi et al.* (2013); *Kollet and Maxwell* (2008)), where cells with a deep water table (over $\sim$ 5m) show lower latent heat and cells with very shallow (under $\sim$ 1m) water table have the highest values in latent heat. In these two extremes, the relation between latent heat and water table depth is weak, and small variations in water table depth to not influence the latent heat flux. Conversely, between these two extremes, the transition zone shows a steep relation between the two variables. This means that a small difference in water table depth results in a large variation in latent heat.

The month of July and the central hour of the day, 13.00, were chosen because of their larger values of latent heat. In the winter months (October to March) there is no definition in the pattern and no S shape is visible. Dif-

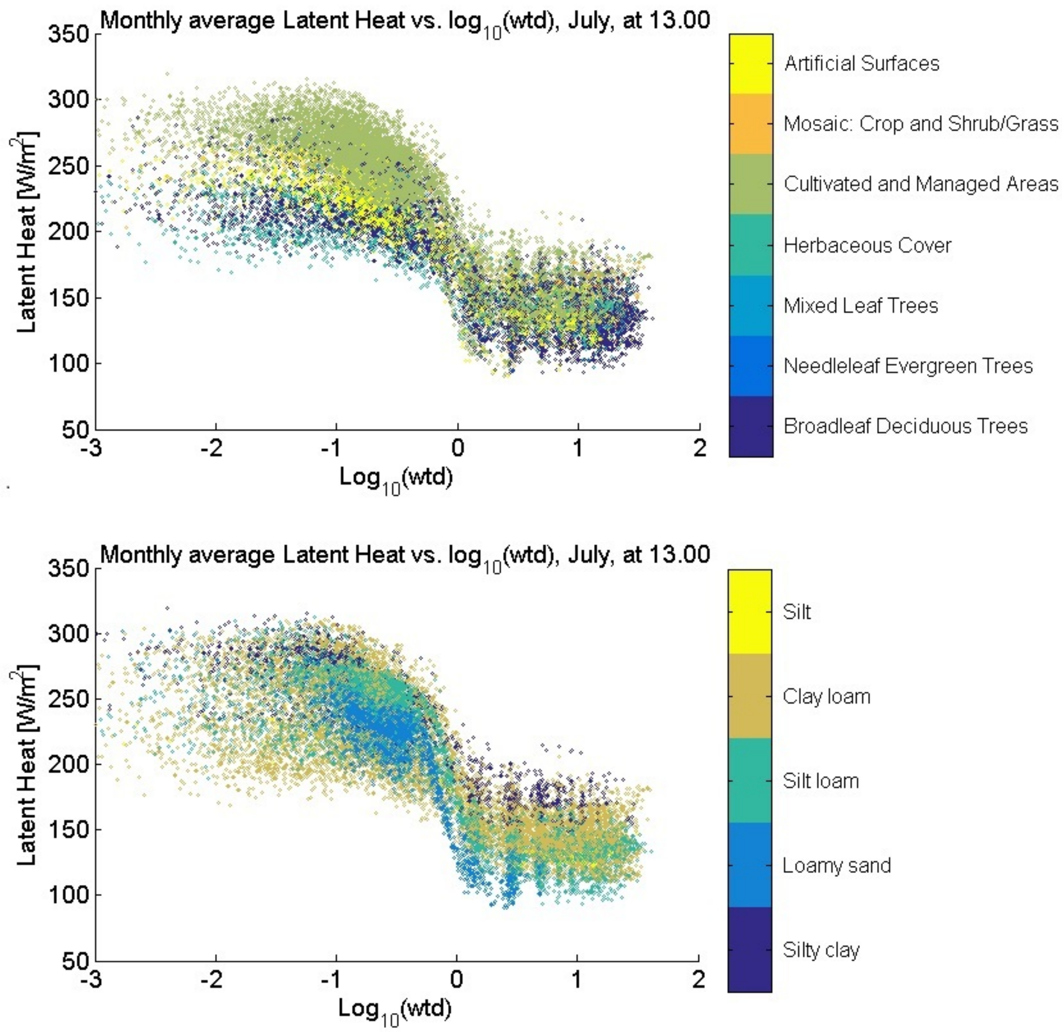

Figure 4. Scatter plot of the monthly average latent heat flux, for the month of July at 13.00, against logarithm of water table depth. The dots represent single cells in the domain and are coloured according to land use (top) and soil texture (bottom). Only cells with $wtd > 10^{-3}$ m are displayed.

ferent land uses and soil textures present different values of latent heat, e.g., the herbaceous cover does not reach the high values shown by vegetation with higher leaf area index. With regard to the soil texture, the values of latent heat for silty clay mostly exceed those found for silt loam and loamy sand. While all these relations can be explained by the different hydraulic conductivities (for the soils) or root depths and leaf area indices (for the vegetation), the position of the cells in the domain also determines the availability of water, whose effect is superposed on the physical characteristics of the land cover and soil texture.

3.1.2 Analysis of the topographic indices

The Topographic Index for the domain is shown in Figure 2. The river channels correspond to the highest values of *TI*, but many other paths are visible, even where the water is not ponded over the surface, that correspond to the directions of the gravity driven water flow in the subsurface.

With respect to *TI*, which increases along the high flow accumulation areas represented by the river channels and, more generally, by converging areas, forming narrow, discrete lines, the DTW index shows a smoother pattern (Figure 2). In particular, DTW increases slowly in the flat northern part of the domain, while the increment is faster in the steeper terrain of the mountainous southern region.

The analysis of $log_{10}(DTW)$ is useful to have a clearer image of the flatter area, where the index increase slowly with the distance from the river. For the similar, although inverted dependence on the slope, the $log_{10}(DTW)$ shows a pattern similar to *TI*. In fact, there is a linear relationship between the two, as shown in Figure 5. The values are averaged using a moving average over squared neighbourhoods of 4*4 cells, as in *Murphy et al.* (2011), in order to remove small-scale variability and get a clearer picture. The red line shows the linear fit, which has a coefficient of determination of ~ 0.81. The inverse relationship

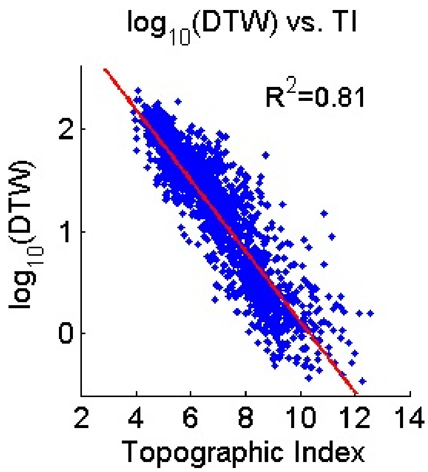

Figure 5. Scatterplot of $\log_{10}(DTW)$ and TI. The variables were previously averaged over 4 cells * 4 cells neighbourhood. The red line shows the linear fit, $\log_{10}(DTW) = -0.34 * TI + 3.57$.

between the two indices is due to the their formulation: the topographic index accumulates the contributing area that is upslope with respect to the cell, while the DTW measures the distance (in height) between the cell and the closest river cell that is downslope. On the other hand, they both use the same algorithm for the determination of the path and both depend on the slope distribution of the catchment (but a logarithm is applied on the TI), which explains the close agreement between them.

3.1.3 Relationship between Latent Heat Flux and Topographic Indices

The topographic wetness index was developed to parameterize the water table depth, and therefore it is related to the soil moisture in the uppermost soil layers. Evapotranspiration is affected by the availability of water in the soil. The relation between water table depth and the land surface energy fluxes has been demonstrated in the past (*Kollet and Maxwell*, 2008) and also shown in Figure 4. For this reason we can expect to find a dependence of latent heat flux

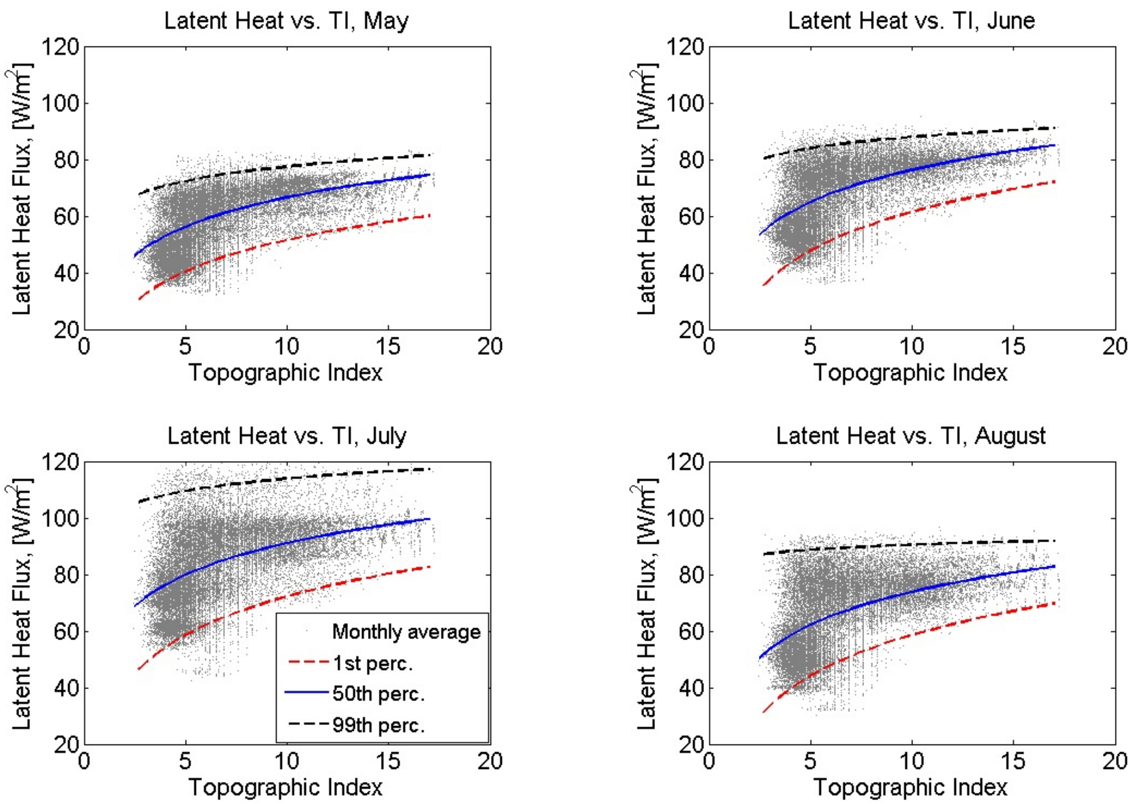

Figure 6. Scatter plot of the monthly average of latent heat against topographic index for the months from May to August. The lines represent the logarithmic fit of the 1st, 50th and 99th percentiles over small intervals of *TI*. Every cell in the domain is represented by its average value over the month.

on the topographic indices, as these are proxies for the water table depth.

Figure 6 show the scatter plots of the monthly average of latent heat flux and the topographic index, for every cell in the domain. Even if the values of latent heat flux show a large scatter for the same value of topographic index, a relationship can be found in the 1st, 50th and 99th percentiles, which were computed over TI bins of size 0.5.

While in winter (not shown here) the radiation is the limiting factor for the evapotranspiration, in summer this happens only for the cells that are not limited in soil moisture. In the case of high topographic index ($TI > 12$), the water table is shallow and there is full availability of water, that can fulfill the atmospheric demand. The flat relationship between the latent heat and TI over a certain threshold reflects the fact that the increment in soil moisture does not automatically reflect into more evapotranspiration and is also consistent with the relationship of latent heat to water table depth (see Figure 4). For low values of topographic index, on the other hand, the water table is deeper, the soil is not saturated and the system is water-limited.

Part of the scatter is due to the overlap of the effects of different kinds of land use, as shown in Figure 7. Each colour corresponds to a different land use class and every class is fitted using a first order Lowess technique, i.e. a locally weighted regression method that reduces the influence of the outliers by smoothing the curve and approximating the trend with local linear trends. Every land use class presents similar trends, but for July the difference is much larger than for the other months. For August, in particular, the water limitation affected all the classes. It is also interesting to notice the different behaviour of the herbaceous cover, which presents a lower latent heat flux, with respect to the different categories of trees (broadleaved deciduous, needleleaf evergreen and mixed leaf trees). Trees can produce higher evapotranspiration even in areas with drier soil, corresponding to low values of topographic index. The deeper root zone allows to reach deeper water tables and higher leaf area index increases the transpiration.

The effect of the land use varies between months and is not always very defined, because the resulting pattern is affected by other factors as well, for example, the atmospheric forcings, such as radiation and precipitation, since those vary within the domain.

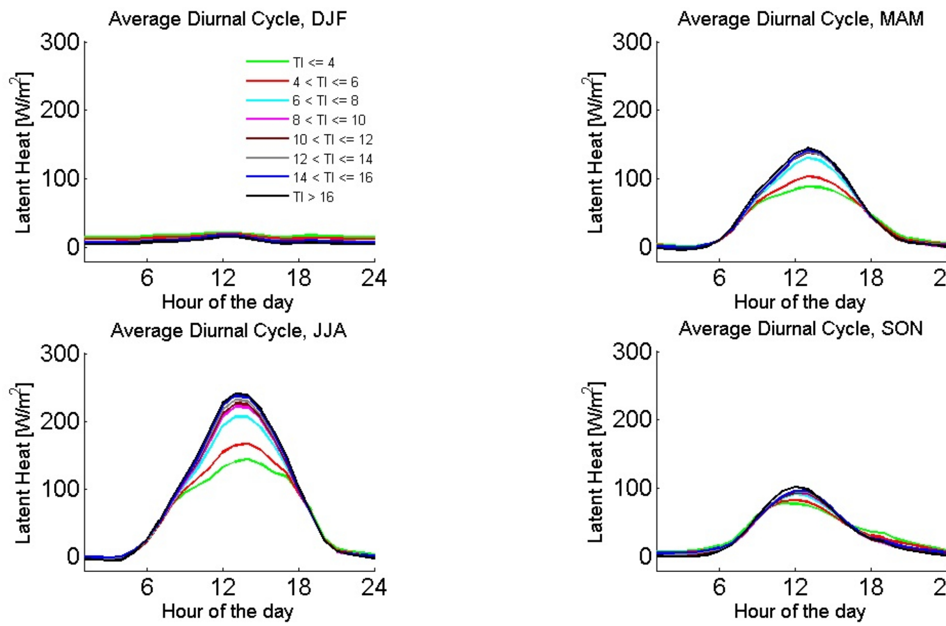

Figure 8. Overview of the seasonal average diurnal cycle of latent heat flux, for the different classes of *TI*.

3.1.4 Seasonal cycle of latent heat flux

Topographic index, as a measure of availability of water, is just one of the possible factors in determining the energy fluxes. Latent heat also has a diurnal and seasonal cycle, that reflects the availability of energy. Figure 8, shows the seasonal average diurnal cycle of latent heat flux for different classes of topographic index during the whole year. In order to obtain a smooth cycle and prevent spikes due to outliers, a 3-hour moving average was applied (see, e.g., *Deshpande and Goswami*, 2014).

The diurnal cycle shows higher values of latent heat for the summer months, in correspondence to the increased incoming radiation, as expected. Moreover, in these months the behaviour of the different classes of *TI* captures a larger variability, with maximum differences between the classes of *TI* of 50% around the middle of the day. This reflects the fact that neither energy nor water

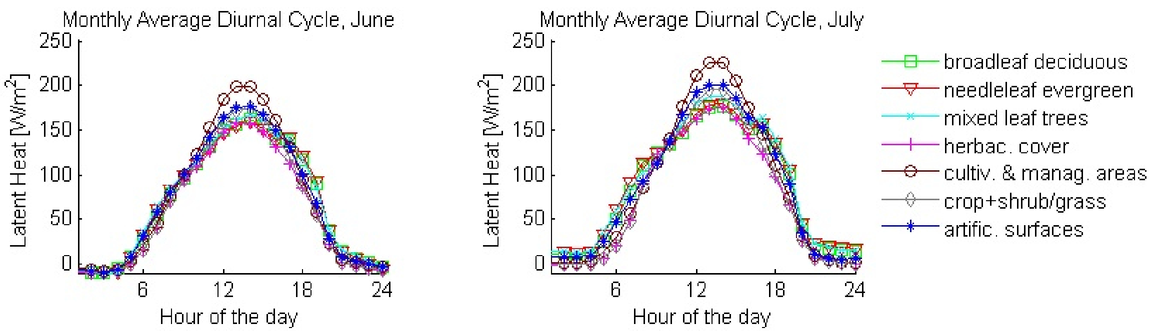

Figure 9. Monthly average diurnal cycle of latent heat flux for different classes of land use, for June and July. Every dot represents the average for one land use class and an hour of the day over the month.

are limited for cells with high TI in conditions of high incoming radiation, and is consistent with the larger dependence of LE on the groundwater during summer (*Rahman et al.*, 2014). During winter, on the other hand, the system is mostly energy-limited in this region of Germany and no real distinction is possible between the different classes of TI. For this reason we mostly focus on the summer months in our analysis.

It should be noted that the dependence on the topographic index does not only reflect a relationship to the hydrodynamics, since land use and soil are also partially correlated to topography (not shown) and are also key factors in LE.

3.1.5 Effect of land use and soil texture

As seen in Figures 6-7, the land use is also affecting the energy fluxes. It not only determines albedo, but is also central in the evapotranspiration processes. Figure 9 shows the diurnal cycle of latent heat for different kinds of land use, for two months. Land use is responsible for differences in the maximum (in the central hours of the day), but some variability is also present under conditions of very low incoming radiation, i.e. in the night hours, where the areas covered by trees show higher latent heat flux.

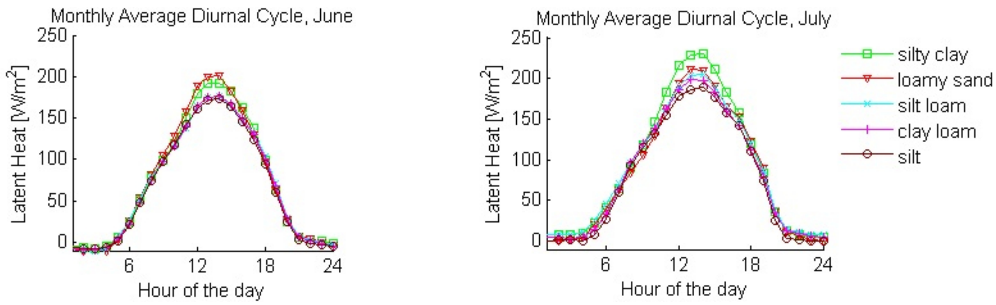

Figure 10. Monthly average diurnal cycle of latent heat flux for different classes of soil, June and July. Every dot represents the average for one soil type and an hour of the day over the month.

Figure 10 shows the monthly average diurnal cycle of latent heat flux filtered for the different soils for two months. The variability is less pronounced than for landuse, and is only present in the central hours of the day. Once again, it is important to notice that the effect of other variables, like landuse and topography, can be confounding factors.

3.1.6 Correlation of topographic index and latent heat flux

The main object of our analysis is the relationship between the topographic indices and the land surface processes and in particular the predictive skills of topographic indices with respect to the energy fluxes, also in comparison with other possible predictors (such as land use and soil texture). In the monthly average diurnal cycle (Figure 11), the topographic index TI shows a clear, direct correlation, i.e. higher values of topographic index correspond to higher values of LE flux for the central hours of the day and the difference between the maximum value for the highest and for the lowest class is larger than the difference between the classes of land use and between the classes of soil. The behaviour of the highest classes of topographic index do not show appreciable differences, since they are above the threshold in topographic index that corresponds to water tables at the surface, and so are virtually not water-limited.

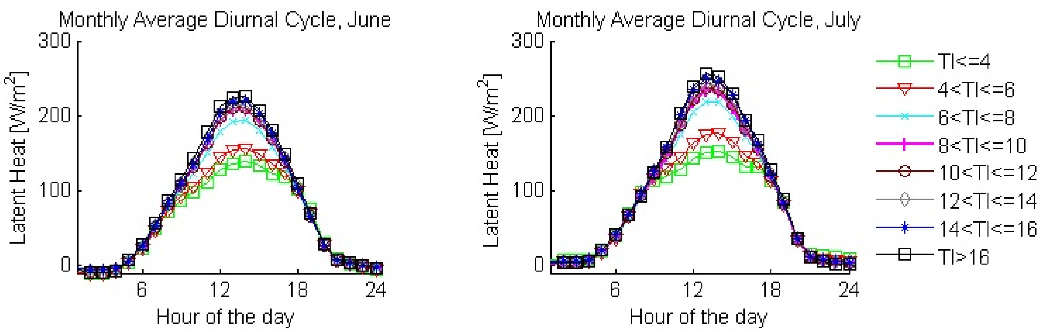

Figure 11. Monthly average diurnal cycle of latent heat flux for different classes of Topographic Index, June and July. Every dot represents the average for a class of *TI* and a hour of the day over the month. A 3 hour-moving average is applied.

This is in agreement with what was found previously in the scatter plots of the monthly average latent heat, but shows also a dependence on the hour of the day and a clear diurnal cycle for every class of *TI*, that was previously not visible. The monthly average diurnal cycles for classes of DTW (not shown) present an analogous pattern, with the classes corresponding to the highest availability of water having the highest *LE*.

3.1.7 Evapotranspiration surplus

In the case of the *PotLERun*, the water abundance in the cells does not depend on the *TI*, since the saturation is kept artificially at the surface. This means that useful information can be extracted from the comparison of the two runs, regarding the different behaviours of the cells in these two setups.

Figure 12 shows the map of the monthly average latent heat and potential latent heat, for July. While the potential latent heat mainly shows the signal of land use, with high values for the tree PFTs and lower values for the herbaceous cover, the latent heat in the *CplxRun* shows also the signal of topography (see Figure 2). For *PotLERun*, where the availability of water is kept artificially at its maximum, this signal is not present.

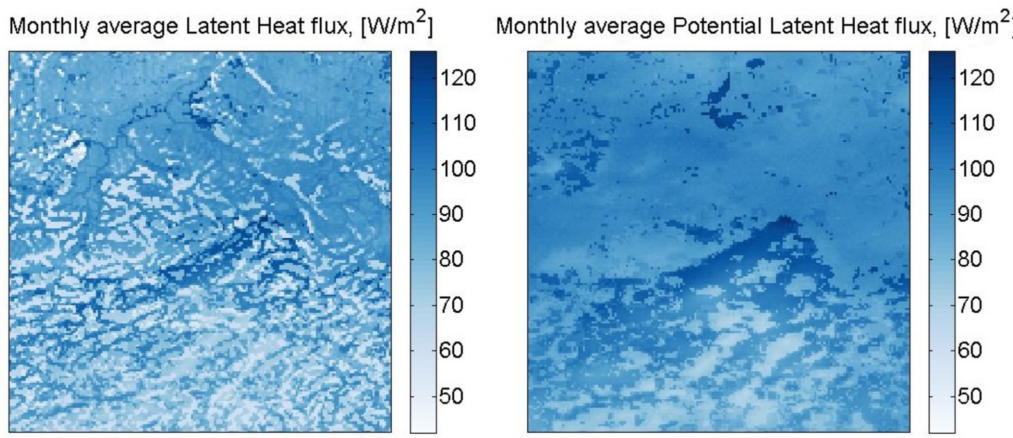

Figure 12. Map of the monthly average latent heat for the month of July, for the *CplxRun* (left) and for the *PotLERun* (right).

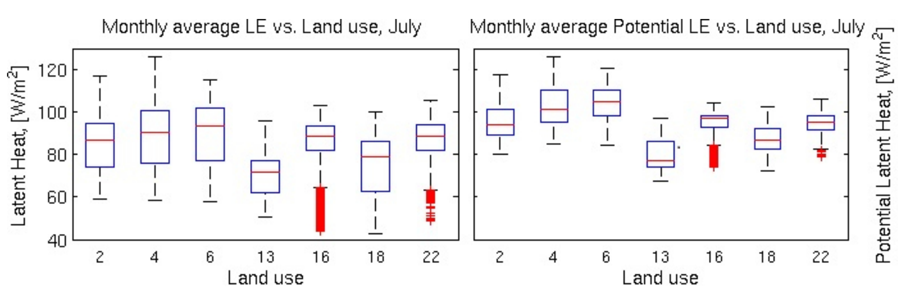

Figure 13. Box plots of the monthly average actual (left) and potential (right) latent heat flux (25th, 50th and 75th percentiles in the box, whiskers up to the most extreme non-outliers points and red crosses for the outliers) for different land uses, for the month of July. For the land use map, the correspondence is: 2) broadleaved deciduous trees; 4) needle-leaved evergreen trees; 6) mixed leaf type trees; 13) herbaceous cover; 16) cultivated and managed areas; 18) mosaic: cropland/shrub or grass cover; 22) artificial surfaces and associated areas.

Figure 13 shows the distributions of actual and potential latent heat flux for the month of July, for the different land use and soil type. In case of the potential latent heat, the first three boxes, that correspond to the tree cover, present the highest values, but this is less clear in the case of the actual latent heat, where the variability is larger because the availability of water also becomes an important factor. Moreover, the distributions are distinctly larger and the (ΔLE) values smaller for every land use in the actual latent heat, where the moisture limitation lowers the evapotranspiration in most of the cells.

We define *evapotranspiration surplus* the difference between the potential and the actual evapotranspiration in a cell, i.e. the evapotranspiration in the case of *CplxRun* and *PotLERun*, respectively.

Figure 14 shows the map of average ΔLE for the month of July. The signal of topographic index (Figure 2) is clearly visible. This is consistent with the fact that the only difference between the two runs is in the availability of water, which is strongly dependent on the topography in one case and kept constant in the other. Negative values of ΔLE, i.e., cells which present a monthly average potential latent heat lower than the actual latent heat, are rare but possible; the higher rate of evapotranspiration causes a drop in temperature that influences the evapotranspiration itself.

As already observed while analyzing the influence of TI on the latent heat, the evapotranspiration is strongly dependent on the availability of water. This is reflected in Figure 15, where the box plots of distributions of ΔLE for the different classes of TI are depicted. At high values of TI correspond no limitation in water and the evapotranspiration depends on the other parameters, first of all the energy. At low values of *TI*, on the other hand, the difference is larger. While the effect is clear for the median values, the spread of the distribution is large, in particular for the most populated classes of *TI.* The same dependence

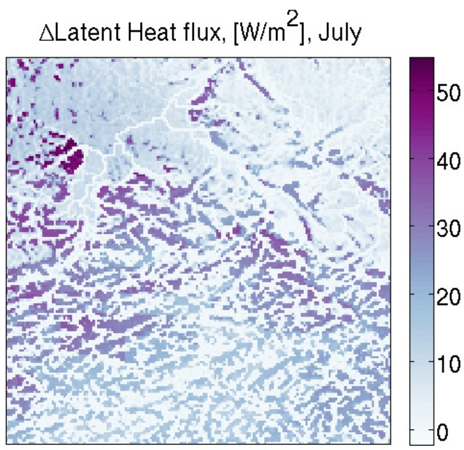

Figure 14. Map of the monthly average ΔLE for July, that clearly shows the signal of the topographic index.

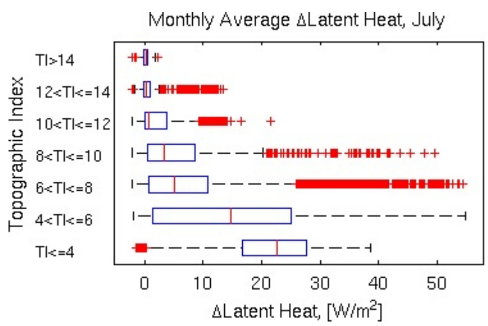

Figure 15. Box plots of the monthly average difference between potential and actual latent heat flux for different land uses, for the month of July.

of ΔLE on TI is present also in Figure 16, where the monthly average diurnal cycle of ΔLE for different classes of TI is shown. During the night, there is no visible difference between the TI classes. For the central hours of the day a clear dependence on the topographic index is visible. While for high values of TI the difference between the runs is close to zero, because the latent heat is at its potential, for low values of TI the difference becomes large, because in the *CplxRun* those cells are water-limited. The variability between the TI classes increases towards summer, with more classes exhibiting non-zero difference.

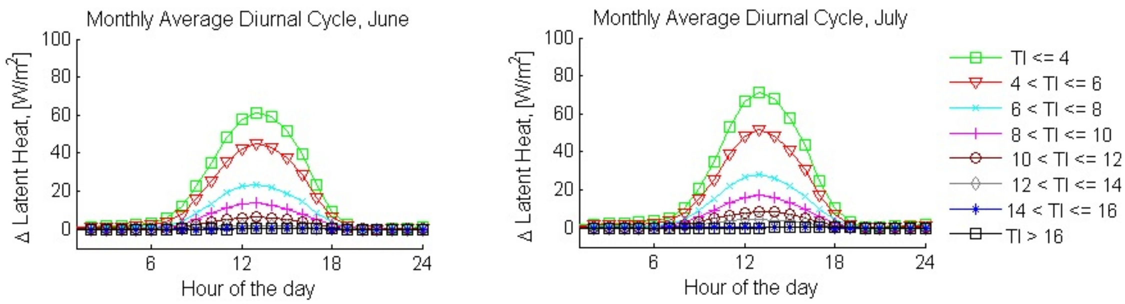

Figure 16. Monthly average diurnal cycle of ΔLE. The curves show the median value for each class of Topographic Wetness Index. A 3h-moving average is applied to the single hour values.

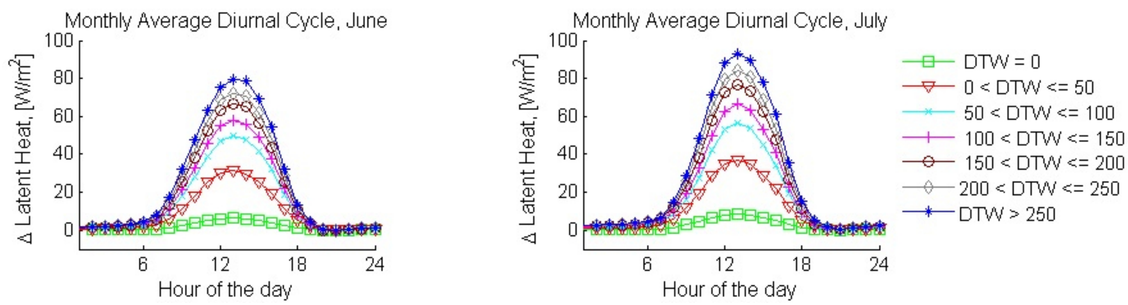

Figure 17. Monthly average diurnal cycle of ΔLE. The curves show the median value for each class of Depth-to-Water.

In Figure 17, the monthly average diurnal cycles for classes of DTW are depicted, for the months of June and July. As expected, and as already shown for TI, the increased availability of water in the classes with lower DTW is reflected in a smaller ΔLE. The difference is maximal when there is less limitation in the radiation (summer months, central hours of the day), while it is aproximately zero during the night (or in the winter months, not shown here).

The shape of the diurnal cycle of ΔLE reflects the dependence on the incoming radiation.

3.2 A model for latent heat flux

3.2.1 Validation method

In order to demonstrate the ability of the topographic indices to quantify the ΔLE, the following procedure was applied. The entire domain was subdivided into two subsets, one for the training and one for the validation of the method. For the training data, the information coming from the *PotLERun* and the characteristics of the cells (e.g., the topographic indices) were used as predictors to develop a model for ΔLE. For validation, the outputs of the *CplxRun* were used.

The two subsets are organized in a "checkers" scheme, where the dark squares represent the training data and the whites are the validation, and vice versa. To ensure independence, the size of the squares needs to be large enough, thus the correlation length of the ΔLE was estimated. The analysis of the variogram shows it to be no larger than 5 km, which means that squares of 21 km of side length are a reasonable choice.

3.2.2 Statistical model

The diurnal cycle on one subset was fitted with a modified Gaussian function,

$$F(t) = A_0 + A * \exp[\frac{-(t-t_0)^2}{2*w}] \tag{7}$$

using an offset A_0, the difference between the maximum and minimum values as height A, $t = 13$ as the central hour, t_0, and a width, w, of 7 hours, for each class of the topographic index. The parameters were estimated by means of a dummy distribution with the same shape as the diurnal cycle over the month of July (where the bell is more pronounced) and checked on the other months.

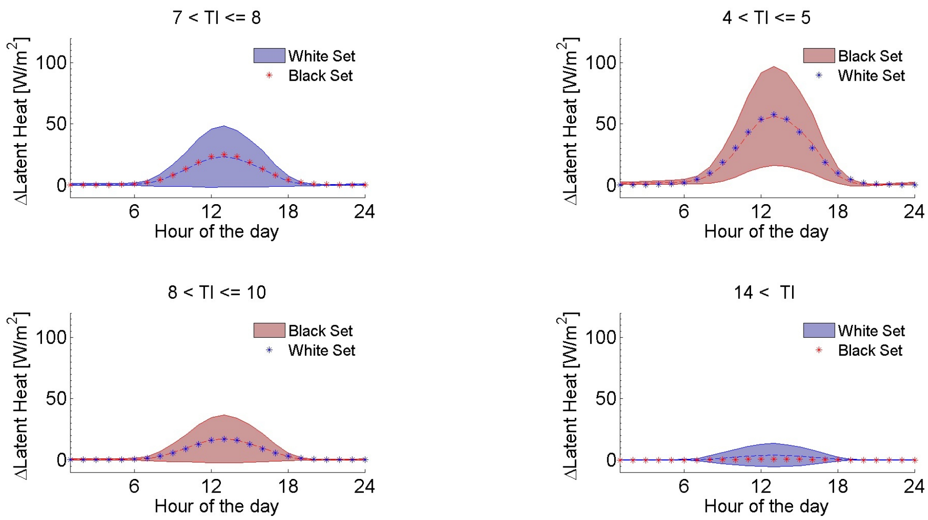

Figure 18. Examples of the comparison between the distribution of values of ΔLE for the black (white) subset of the domain -i.e. the validation subset- and the bell calculated on the white (black) subset for the same class of TI - i.e. the training subset. The dashed line represents the mean for the class and the filled area gives the standard deviation of the model. The stars show the values predicted for that hour and that class of *TI*, based on the corresponding data in the other subset.

3.2.3 Validation results

The plots in Figure 18 depict some examples of the monthly average diurnal cycles of ΔLE for a single class of *TI*. In order to represent the distribution of values, the mean (dashed line) and an interval of two standard deviations are displayed. The value predicted based on the information provided by the other subset are added for comparison (stars). In most of the cases, the function developed on one subset is able to reproduce he mean well in its counterpart, but some TI classes exhibit a large spread.

Similarly, in Figure 19 some examples of the monthly average diurnal cycles of ΔLE for single classes of DTW are depicted. As for the *TI*, also DTW is able to catch the average behaviour in each class fairly well, but the spread in

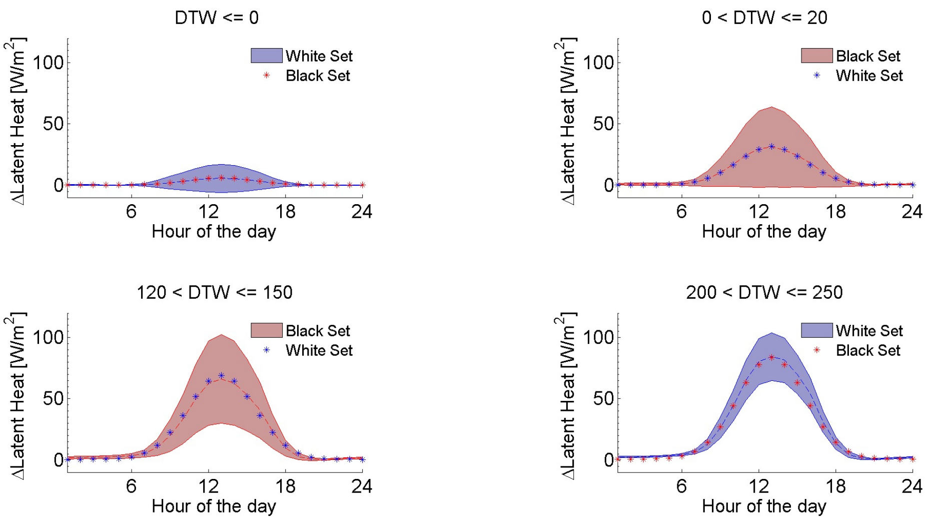

Figure 19. Examples of the comparison between the distribution of values of ΔLE for the validation subset and the bell calculated on the training subset. The dashed line represents the mean for the class and the filled area gives the standard deviation of the model. The stars show the values predicted for that hour and that class of DTW, based on the training subset.

the distributions is quite large.

When the value at the central hour is captured correctly, Equation 7 represents fairly well the values during the rest of the day. The central hour is also the timestep were the spread in the classes is largest. Figure 20 shows the map of the difference between the values of monthly average ΔLE predicted by the model and those simulated in the *CplxRun*, in the central hour of the day, for the model based on TI (left) and DTW (right). While the mean over the domain is close to zero in both cases, a clear pattern is present. Both negative and positive values are present (indicating, respectively, under- and overestimation of the latent heat flux), with mostly small scale structures in the southern part and a region with very high errors in both the models.

In order to study the origin of the larger scale structures in the bias, its relationship to the different landuses and soil composition was analyzed. In

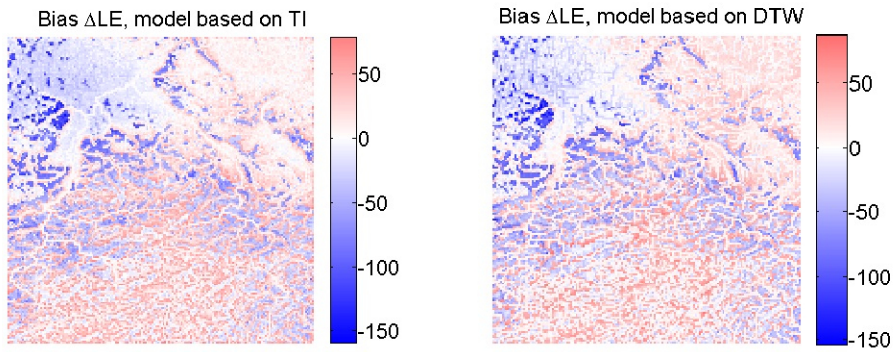

Figure 20. Maps of the difference between the monthly average values of ΔLE predicted and the values obtained from the simulation, for the central hour (13:00) of the day and the month of July. The prediction is based on TI and on DTW, respectively.

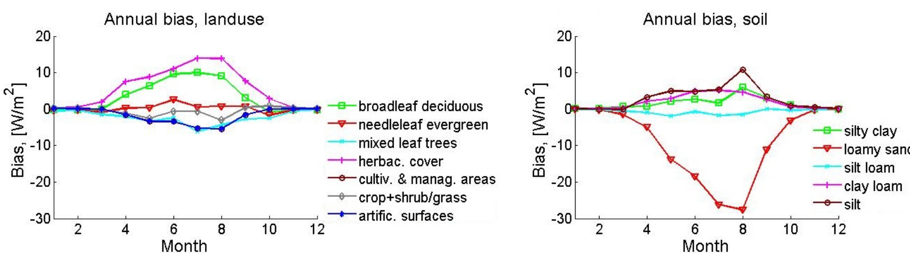

Figure 21. Plot of the mean bias of every class of landuse (left) and soil (right), for each month of the year at 13.00.

Figure21 , the annual trend of the prediction bias (based on TI) of the different classes is depicted, for both landuse and soil. While all the different landuses show comparable results, one of the soil types, loamy sand, presents a very high negative bias for the all summer months. This is in agreement with the large scale structure in the map of bias (Figure 20)

As an alternative form of validation, the results of the statistical model were tested against a free-drainage (FD) simulation (*Rahman et al.*, 2016). While this kind of land surface model is known to be a strong simplification, it still represents a widely used approach. The range of the error is equally large, yet the FD run shows a localized bias and poorly captures the spatial mean.

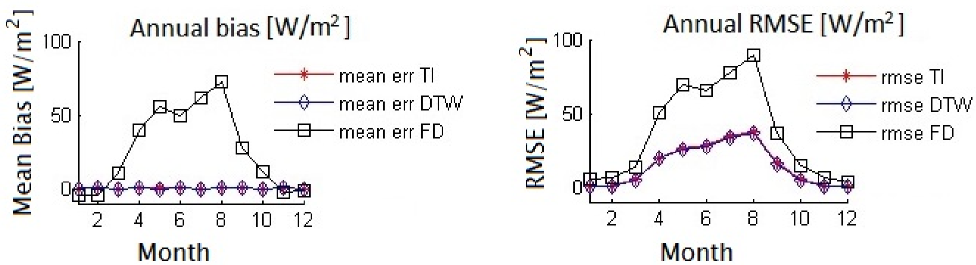

Figure 22. Comparison of the annual cycle of the root mean square error (left) and mean bias (right) for the free drainage simulation and the statistical models based on TI and DTW, at 13.00, for the monthly averages of LE.

The comparison of the root mean square error for the models (Figure 22) shows similar performances for the two statistical models, and a better performance compared to the free-drainage simulation. The choice of the central hour of the day is meant to serve as a worst case scenario, since that is the condition where the error is maximal. The fact that the bias is close to zero is a confirmation of the assumption that the mean ΔLE for the classes is representative of the value for the single cells. This means that it is possible to predict the values for areas where only the simplified model was run, based on the class of topographic indices and the results of the full simulation in the training set, and to obtain an accurate spatial mean that can be provided as boundary condition to larger scale models.

4 Summary and conclusions

Groundwater is an important factor for the simulation of the energy fluxes at the land surface. Unfortunately, a full-physics representation of the subsurface hydrodynamics is mostly not feasible for climate simulations with long runs or large domains. We propose an approach that reduces the computational burden, by using a parameterized run and corrections based on the sensitivities of the energy fluxes, and in particular of the latent heat flux, to topographic indices.

Two sets of simulations where used in the development of the model. The first simulation, *CplxRun*, is a full-physics simulation, the results of which represent the true values of the variables. The second simulation, Potential Latent Heat Run, *PotLERun*, is a highly parameterized version, where the water table depth is artificially kept close to saturation. This serves the purpose of saving computational time and shedding light on the behaviour of non water-limited cells, since the influence of the water availability is subtracted.

From the analysis of the results of the *CplxRun*, it is visible how the latent heat flux is strongly influenced by the availability of energy, as shown by the dependence on the time of the year and hour of the day, and by the availability of water. When the incoming radiation is not sufficient to trigger the evapotranspiration (in the winter months and in the night hours all over the seasons), the latent heat flux is close to zero and no evapotranspiration is present even for the *PotLERun,* despite the major water content in the soil. Even in the case of full availability of water, this does not translate into a systematic increase in evapotranspiration (Figure 6), since the energy is also a limiting factor.

Through the comparison of the latent heat in the *CplxRun* to its counterpart under conditions of full saturation (*PotLERun*), we were able to isolate the effect of the topographic indices and develop a statistical model to calculate the actual LE from the results of a parameterized run. The two topographic indices, the Topographic Index*, TI,* and Depth-To-Water, DTW, because of their relationship to the water table depth, are good proxies for the water availability, and show in general a significant effect on the diurnal cycle of latent heat flux, with respect to the land use and soil texture. The average diurnal cycles for the different classes of TI present a constant pattern over the year (Figure 8), where the high values of TI are related to the higher values of latent heat flux. While the relationship between latent heat flux and topographic indices exhibits too much scatter to be able to establish a simple mathematical relationship with sufficient confidence, it was possible to develop a statistical model for the determination of the maximal value of the difference in evapotranspiration, ΔLE, corresponding to the central hour of the day, for each class of the predictor (TI or DTW). This value was then used to fit the top of the bell that represented the diurnal cycle.

The difference in latent heat between the two runs, evapotranspiration surplus (ΔLE) shows a marked relationship to the topographic indices (Figure 16), since everything is kept constant between the two simulations, except for the position of the water table. This means that the availability of water and all the quantities that derive from it, are well represented in the difference. The diurnal cycle of ΔLE for the classes of TI and DTW shows a bell shape, with the highest classes of TI and lowest classes of DTW presenting the lowest values of ΔLE (since they approximate their full potential in moisture).

The diurnal cycle for every class was then fitted with a modified Gaussian bell, that reproduces fairly well the diurnal cycle of ΔLE. While the mean values for each class are well behaved and are ordered according to the topographic index, the spread in some of the classes is very large. This is due to the fact that topography is not the only parameter influencing the surface energy fluxes. While part of the information about landuse and soil, for example, is present in the topographic indices, for the natural relationship between topography and surface characteristics, part of it is lost.

The validation of the method, through the extraction of two subsets and the comparison of the results obtained on the training subset to the distributions of value on the validation subset, showed a good agreement in the values of the mean. The domain was subdivided into two subdomains. Under the assumption that the topographic indices are good predictors for the ΔLE, the bell fitted on the mean for each class of topographic index in one subset was superimposed to the distribution of the same classes on the second subset. The possibility of dividing the domain into two regions (east-west or north-south) was explored and had to be discarded. The major objection against the north-south subdivision was due to the deeply different average elevation, the southern area being mostly over 400 m.a.s.l. and the northern region being mostly flat and around 200 m.a.s.l., and the related different precipitation rate. For the east-west subdivision, the major concern was due to the different soil texture, and in particular with the loamy sand being only present on one side of the domain. The subdivision into two checkers subsets was able to capture the general trend and to avoid discrepancies due to large scale trends, but showed mixed results. While the model developed in the training subset was able to reproduce the mean in the validation subset very well, for some of the classes the spread was very large and this translated into large errors in the prediction of the ΔLE.

The two predictors, TI and DTW, do not show appreciable difference in the root mean square errore and bias, but exhibit some differences in the spatial distribution. This is in agreement with the common basis of the two indices on the slopes. When compared against the free drainage run, results of a simulation where the soil moisture is allowed to leave the domain via gravity drainage, the statistical model performs satisfactorily, both in the winter and summer months. The low mean bias of the statistical model, in particular, indicates that the spatial mean of the predicted latent heat flux is a good approximation of the results provided by the full-physics model. In particular, the spatial mean could be provided to *GCMs* or *RCMs* as the lower boundary flux and would represents an improvement with respect to the free-drainage run.

Future work will substitute the discrete classes with continuous functions, which will allow to reproduce the differences that are now neglected inside the classes and, in particular, the steep increment of latent heat flux for low values of topographic index *TI*. Further improvement may be achieved with an optimization of the fit of the diurnal cycle (e.g., via a machine learning approach for the estimation of the parameters over the different months). In an application, the *CplxRun* would only be used to model small catchments in a part of the full modelling area. Finally, an implementation of the concept over time should be explored, with a statistical model based also on the atmospheric forcing. This would allow to overcome the difficulties posed to the generalization of the results by the heterogeneity in soil and landuse.

References

Alley, W. M., R. W. Healy, J. W. LaBaugh, and T. E. Reilly, Flow and Storage in Groundwater Systems, *Science*, *296*, 2002.

Anyah, R. O., C. P. Weaver, G. Miguez-Macho, Y. Fan, and A. Robock, Incorporating water table dynamics in climate modeling: 3 . Simulated groundwater influence on coupled land-atmosphere variability, *Journal of Geophysical Research*, *113*, 1–15, 2008.

Betts, A. K., Understanding Hydrometeorology using Global Models, *Bull. Amer. Meteor. Soc.*, *85*, 1673–1688, 2004.

Beven, K., *Runoff Production and Flood Frequency in Catchments of Order n: An Alternative Approach*, pp. 107–131, Springer Netherlands, Dordrecht, 1986.

Beven, K., TOPMODEL: A critique, *Hydrol. Process.*, *11*, 1069–1085, 1997.

Beven, K. J., and M. J. Kirkby, a physically based, variable contributing area model of basin hydrology, *Hydrological Sciences Bulletin*, *24*, 1979.

Beven, K. J., M. J. Kirkby, N. Schofield, and A. F. Tagg, Testing a physically-based flood forecasting model (TOPMODEL) for three U.K. catchments, *Journal of Hydrology*, *69*, 119–143, 1984.

Choi, H. I., and X.-Z. Liang, Improved terrestrial hydrologic representation in mesoscale land surface models, *Journal of Hydrometeorology*, *11*, 797–809, 2010.

Chou, C., and J. D. Neelin, Mechanisms of Global Warming Impacts on Regional Tropical Precipitation, *Journal of Climate*, *17*, 2688–2701, 2004.

Decker, M., A. J. Pitman, and J. P. Evans, Groundwater Constraints on Simulated Transpiration Variability over Southeastern Australian, *Journal of Hydrometeorology*, *14*, 543–559, 2013.

Deshpande, N. R., and B. N. Goswami, Modulation of the diurnal cycle of rainfall over India by intraseasonal variations of Indian summer monsoon, *International Journal of Climatology*, *34*, 793–807, 2014.

Dingman, S. L., *Physical Hydrology*, Upper Saddle River, NJ, Prentice Hall, 2002.

Ducharne, A., Reducing scale dependence in TOPMODEL using a dimensionless topographic index, *Hydrology and Earth System Sciences*, *13*, 2399–2412, 2009.

Fan, Y., Groundwater in the Earth's critical zone: Relevance to large-scale patterns and processes, *Water Resources Research*, *51*, 3052–3069, 2015.

Fan, Y., and G. Miguez-Macho, Potential groundwater contribution to Amazon evapotranspiration, *Hydrol. Earth Syst. Sci.*, *14*, 2039–2056, 2010.

Ferguson, I. M., and R. M. Maxwell, Role of groundwater in watershed response and land surface feedbacks under climate change, *Water Resources Research*, *46*, 1–15, 2010.

Franchini, M., J. Wendling, C. Obled, and E. Todini, Physical interpretation and sensitivity analysis of the TOPMODEL, *J. Hydrol.*, *175*, 1996.

Gleick, P. H., *Water In Crisis: a Guide to the World's Fresh Water Resources*, New York: Oxford University Press, 1993.

Greve, P., B. Orlowsky, B. Mueller, J. Sheffield, M. Reichstein, and S. I. Seneviratne, Global assessment of trends in wetting and drying over land, *Nature Geoscience*, *7*, 716–721, 2014.

Hjerdt, K. N., J. J. McDonnell, J. Seibert, and A. Rodhe, A new topographic index to quantify downslope controls on local drainage, *Water Resources Research*, *40*, 1–6, 2004.

Jiang, X., G.-Y. Niu, and Z.-L. Yang, Impacts of vegetation and groundwater dynamics on warm season precipitation over the Central United States, *Journal of Geophysical Research*, *114*, 1–15, 2009.

Koirala, S., P. J.-F. Yeh, Y. Hirabayashi, S. Kanae, and T. Oki, Global-scale land surface hydrologic modeling with the representation of water table dynamics, *Journal of Geophysical Research*, *119*, 75–89, 2014.

Kollet, S. J., and R. M. Maxwell, Integrated surface-groundwater flow modeling: a free-surface overland flow boundary condition in a parallel groundwater flow model, *Advances in Water Resources*, *29*, 945–958, 2006.

Kollet, S. J., and R. M. Maxwell, Capturing the influence of groundwater dynamics on land surface processes using an integrated, distributed watershed model, *Water Resources Research*, *44*, 1–18, 2008.

Lam, A., D. Karssenberg, B. J. J. M. van den Hurk, and M. F. P. Bierkens, Spatial and temporal connections in groundwater contribution to evaporation, *Hydrol. Earth Syst. Sci.*, *15*, 2621–2630, 2011.

Leng, G., M. Huang, Q. Tang, H. Gao, and L. R. Leung, Modeling the effects of groundwater-fed irrigation on terrestrial hydrology over the conterminous United States, *Journal of Hydrometeorology*, *15*, 957–972, 2014.

Leung, L. R., M. Huang, Y. Qian, and X. Liang, Climate-soil-vegetation control on groundwater table dynamics and its feedbacks in a climate model, *Climate Dynamics*, *36*, 57–81, 2011.

Lo, M.-H., and J. S. Famiglietti, Effect of water table dynamics on land surface hydrologic memory, *Journal of Geophysical Research-Atmospheres*, *115*, 2010.

Lo, M.-H., and J. S. Famiglietti, Precipitation response to land subsurface hydrologic processes in atmospheric general circulation model simulations, *Journal of Geophysical Research*, *116*, 2011.

Manners, J., J.-C. Thelen, J. Petch, P. Hill, and J. Edwards, Two fast radiative transfer methods to improve the temporal sampling of clouds in numerical weather prediction and climate models, *Quarterly Journal of the Royal Meteorological Society*, *135*, 457–468, 2009.

Maxwell, R. M., and S. J. Kollet, Interdependence of Groundwater Dynamics and Land-Energy Feedbacks Under Climate Change, *Nature Geoscience*, *1*, 2008.

Maxwell, R. M., and N. L. Miller, Development of a coupled land surface and groundwater model, *Journal of Hydrometeorology*, *6*, 233–247, 2005.

Maxwell, R. M., F. K. Chow, and S. J. Kollet, The groundwater–land-surface–atmosphere connection: soil moisture effects on the atmospheric boundary layer in fully-coupled simulations, *Advances in Water Resources*, *30*, 2447–2466, 2007.

Merot, P., H. Quividant, P. Aurousseau, M. Hefting, T. Burt, V. Maitre, M. Kruk, A. Butturini, C. Thenail, and V. Viaud, Testing a climato-topographic index for predicting wetlands distribution along an European climate gradient, *Ecological Modelling*, *163*, 51–71, 2003.

Miguez-Macho, G., Y. Fan, C. P. Weaver, R. Walko, and A. Robock, Incorporating water table dynamics in climate modeling: 2. Formulation, validation, and soil moisture simulation, *Journal of Geophysical Research*, *112*, 1–16, 2007.

Murphy, P. N. C., J. Ogilvie, K. Connor, and P. A. Arp, Mapping wetlands: a comparison of two different approaches for New Brunswick, Canada, *Wetlands*, *27*, 846–854, 2007.

Murphy, P. N. C., J. Ogilvie, and P. Arp, Topographic modelling of soil moisture conditions: a comparison and verification of two models, *European Journal of Soil Science*, *60*, 94–109, 2009.

Murphy, P. N. C., J. Ogilvie, F.-R. Meng, B. White, J. S. Bhatti, and P. A. Arp, Modelling and mapping topographic variations in forest soils at high resolution: A case study, *Ecological Modelling*, *222*, 2314–2332, 2011.

Niu, G.-Y., Z.-L. Yang, R. E. Dickinson, L. E. Gulden, and H. Su, Development of a simple groundwater model for use in climate models and evaluation with Gravity Recovery and Climate Experiment data, *J. Geophys. Res.*, *112*, 2007.

Rahman, M., M. Sulis, and S. J. Kollet, The concept of dual-boundary forcing in land surface-subsurface interactions of the terrestrial hydrologic and energy cycles, *Water Resources Research*, *50*, 8531–8548, 2014.

Rahman, M., M. Sulis, and S. J. Kollet, Evaluating the dual-boundary forcing concept in subsurface-land surface interactions of the hydrological cycle, *Hydrological Processes*, *30*, 1563–1573, 2016.

Rennó, D. C., A. D. Nobre, L. A. Cuartas, J. Vianei Soares, M. G. Hodnett, J. Tomasella, and M. J. Waterloo, HAND, a new terrain descriptor using SRTM-DEM: Mapping terra- firme rainforest environments in Amazonia, *Remote Sensing of Environment*, *112*, 3469–3481, 2008.

Rinderer, M., H. J. van Meerveld, and J. Seibert, Topographic controls on shallow groundwater levels in a steep, prealpine catchment: When are the TWI assumptions valid?, *Water Resour. Res.*, *50*, 6067–6080, 2014.

Schomburg, A., V. Venema, F. Ament, and C. Simmer, Application of an adaptive radiative transfer scheme in a mesoscale numerical weather prediction model, *Quarterly Journal of the Royal Meteorological Society*, *138*, 91–102, 2012.

Skalsky, R., Z. Tarasovicov, J. Balkovic, E. Schmid, M. Fuchs, E. Moltchanova, G. Kindermann, and P. Scholtz, GEO-BENE global database for bio-physical modeling v. 1.0, *Geobene Public Research Documents*, 2009.

Soylu, M. E., E. Istanbulluoglu, J. D. Lenters, and T. Wang, Quantifying the impact of groundwater depth on evapotranspiration in a semi-arid grassland region, *Hydrology and Earth System Sciences*, *15*, 787–806, 2011.

Szilagyi, J., V. A. Zlotnik, and J. Jozsa, Net recharge vs. depth to groundwater relationship in the Platte River Valley of Nebraska, United States., *Ground Water*, *51*, 945–951, 2013.

Tian, W., X. Li, G.-D. Cheng, X.-S. Wang, and B. X. Hu, Coupling a groundwater model with a land surface model to improve water and energy cycle simulation, *Hydrol. Earth Syst. Sci.*, *16*, 4707–4723, 2012.

Venema, V., A. Schomburg, F. Ament, and C. Simmer, Two adaptive radiative transfer schemes for numerical weather prediction models, *Atmospheric Chemistry and Physics*, *7*, 5659–5674, 2007.

Vergnes, J.-P., B. Decharme, R. Alkama, E. Martin, F. Habets, and H. Douville, A simple groundwater scheme for hydrological and climate applications: description and offline evaluation over France, *Journal of Hydrometeorology*, *13*, 1149–1171, 2012.

Vergnes, J.-P., B. Decharme, and F. Habets, Introduction of groundwater capillary rises using subgrid spatial variability of topography into the ISBA land surface model, *Journal of Geophysical Research: Atmospheres*, *119*, 11,065–11,086, 2014.

Western, A. W., R. B. Grayson, G. Blöschl, G. R. Willgoose, and T. A. McMahon, Observed spatial organization of soil moisture and its relation to terrain indices, *Water Resources Research*, *35*, 797–810, 1999.

Yeh, P. J.-F., and E. A. B. Eltahir, Representation of water table dynamics in a land surface scheme. Part I: Model development, *Journal of Climate*, *18*, 1861–1880, 2005a.

Yeh, P. J.-F., and E. A. B. Eltahir, Representation of water table dynamics in a land surface scheme. Part II: Subgrid variability, *Journal of Climate*, *18*, 1881–1901, 2005b.

York, J. P., M. Person, W. J. Gutowski, and T. C. Winter, Putting aquifers into atmospheric simulation models: an example from the Mill Creek Watershed, Northeastern Kansas, *Advances in Water Resources*, *25*, 221–238, 2002.

Yuan, X., Z. Xie, J. Zheng, X. Tian, and Z. Yang, Effects of water table dynamics on regional climate: A case study over east Asian monsoon area, *Journal of Geophysical Research*, *113*, 2008.